# Neuro Inspired Computing with Coupled Relaxation Oscillators

Suman Datta[1], Nikhil Shukla[1], Matthew Cotter[1], Abhinav Parihar[2], Arijit Raychowdhury[2]

[1]Department of Electrical Engineering
Penn State University
N-231 Millennium Science Complex, University Park, PA 16802
Contact Email: sdatta@engr.psu.edu

[2]Department of Electrical and Computer Engineering
Georgia Institute of Technology
266 Ferst Drive, Atlanta, GA-30332
Contact Email: arijit.raychowdhury@ece.gatech.edu

## ABSTRACT

***Harnessing the computational capabilities of dynamical systems has attracted the attention of scientists and engineers form varied technical disciplines over decades. The time evolution of coupled, non-linear synchronous oscillatory systems has led to active research in understanding their dynamical properties and exploring their applications in brain-inspired, neuromorphic computational models. In this paper we present the realization of coupled and scalable relaxation-oscillators utilizing the metal-insulator-metal transition of vanadium-dioxide ($VO_2$) thin films. We demonstrate the potential use of such a system in pattern recognition, as one possible computational model using such a system.***

## 1. INTRODUCTION

Ubiquitous, high-fidelity, compact and multi-modal data acquisition devices compounded with increasing device-to-device connectivity have contributed to an overwhelming deluge of data; with an estimated 50 Trillion GB of data residing on more than 30 Billion connected devices by 2020. Although the collection and transmission of data continues to become cheaper both in resources and cost, meaningful analysis of the collected data continues to be a significant challenge. While Boolean, Von-Neumann machines have fueled the technology revolution over the last three decades, it is well recognized that brain-inspired computational models are better suited for tasks such as data classification and recognition. However, such models, like artificial neural networks or convolutional neural networks, are always mapped onto digital computing systems where both performance and power constraints ultimately limit their applicability. The benefits of technology scaling cannot keep up with the data deluge creating an unbridgeable gap between the computational demand and the capability of systems over the next ten years. This requires a transformative approach to explore non-conventional electron devices beyond the CMOS technology. In this paper we propose to harness collective dynamics of carriers in correlated materials and investigate non-Boolean information processing architectures, which fundamentally embraces the "let physics do the computing" paradigm.

Modeling, analysis and design of dynamical systems have captured the imagination of mathematicians, physicists, computer scientists and electrical engineers alike. In one such embodiment of dynamical systems, it has been theoretically demonstrated that synchronized oscillatory systems have unique associative computational capabilities [1]. Implementation of such ideas using STO based coupled systems has been discussed in [2] [3] [4] [5].


*DAC '14*, June 01 - 05 2014, San Francisco, CA, USA

http://dx.doi.org/10.1145/2593069.2596685

Synchronized oscillations are omnipresent and have fascinated scientists through the ages: from the rhythmic firings of groups of fireflies, circadian rhythms in plants and animals to the neuro-oscillators responsible for the human nervous system. Harnessing their computational capabilities can open up new avenues for neuro-morphic computation. Although efforts in building such systems with CMOS components have been undertaken, concerns of scalability in size, power and performance have always been paramount. Consequently such transformative computational paradigms have always lagged the capabilities for CMOS Boolean computational platforms. However, in the last few years nano-oscillator based computing paradigms have gained immense traction as new materials have unraveled possibilities of not only realizing scalable, compact, low-power and high-performance oscillators; but also means of coupling multiple oscillators in a controlled and programmable manner. Of particular interest are spin-torque oscillators (STOs) coupled with spin diffusion current [6] with electrical read-out. In spite of their novelty and scalability, coupled STOs suffer from high bias currents (in the order of mA) and slower speeds that are limited by the angular spin precession velocity in nano-magnets. Further, coupling via spin-diffusion current is low power, but localized as the spin diffusion lengths are in the order of μm in room-temperature. Research has started in the earnest to find alternative nano-oscillator topologies that are scalable and preferably electrically coupled. Recent advances in the manufacturability of systems of complex oxides capable of performing spontaneous metal-insulator-metal transitions under the application of a critical electric field (or, temperature) have generated interest in their applicability in realizing systems of coupled nano-oscillators. In this paper we show though experimental results, mathematical descriptions, and numerical techniques the possibility of realizing such a bio-inspired neuro-computer capable of performing matching. Here we present locking of coupled oscillators as a computational primitive capable of performing associative matching. This, by no means, in the only computational paradigm possible with a system of coupled oscillators. Both phase and frequency control in a system of synchronized oscillators is possible when properly stimulated, programmed and observed.

This paper is divided into the following sections. In Section 2, Vanadium-dioxide ($VO_2$) is presented as a prototypical correlated complex oxide material capable of performing metal-insulator-metal transitions. Sections 3 to 6 describe the theory and experimental results for realization of nano-oscillators using $VO_2$. Electrical coupling in $VO_2$ oscillators and numerical techniques to analyze such a dynamical system is presented in Section 8. Section 9 illustrates the application of pairwise coupling of $VO_2$ oscillators in pattern matching as applied to automatic character recognition. Finally, key results and observations are summarized in Section 10.

## 2. $VO_2$ AS CORRELATED ELECTRON SYSTEM

$VO_2$ is a transition metal oxide that has been of prolonged research interest because of the insulator-metal transition that occurs in this

material, usually just above room temperature (~340K). This phase transition is associated with a large and abrupt change in conductivity up to five orders in magnitude [7] along with a simultaneous structural change. It can be triggered using various external stimuli including thermal [8], electrical [9][10], optical [11] and strain (mechanical) [12] and it has been shown that such a phase transition can be triggered on an ultra-fast time femto-second time scale [11]. The exact physics driving this phase transition has been the subject of a forty year long debate with the principle contenders being the Mott[10][13][14] and the Peierls[15][16] mechanism with some researchers suggesting a weighted contribution from both [17]. In spite of this debate, the exciting electronic property of a large change in conductivity as well as the ultra-fast time scales associated with this transition means that the paradigm of research in this material has evolved from purely academic curiosity to pursuit of real-world device applications based; several optical devices, hybrid-metamaterials and electronic components [18] have been proposed and demonstrated. In the first half of the paper we explore the possibility of realizing $VO_2$ based relaxation oscillators by harnessing these properties.

## 3. $VO_2$ OSCILLATOR CIRCUIT AND DEVICE FABRICATION

The $VO_2$ oscillator consists of a two terminal $VO_2$ device in series with a resistor $R_S$ as shown in Figure 1a. The series resistor provides a negative feedback and its role will be explained in the following sections. The $VO_2$ two terminal devices are fabricated on 17.7 nm ultrathin $VO_2$ films. The $VO_2$ films are epitaxially grown on a $TiO_2$ (001) substrate employing reactive oxide molecular-beam epitaxy. Due to epitaxial mismatch, the $VO_2$ films are biaxially strained in compression by -0.9%. The compressive strain reduces the phase transition temperature of $VO_2$ from 340K to ~310K. First, the electrodes are patterned using contact lithography followed by electron beam evaporation of metal electrodes. Next the channel width and isolation are defined by electron beam lithography followed by a halogen based dry etch. Unless stated otherwise, all electrical measurements reported are performed near room temperature (18°C). The relatively simple device structure and fabrication flow will allow for easier device scaling and high packing density for such devices.

## 4. $VO_2$ OSCILLATOR PRINCIPLE AND OPERATION

The electrically driven insulator-metal transition in $VO_2$ is abrupt, but comes at the expense of a hysteresis. When electrically driven

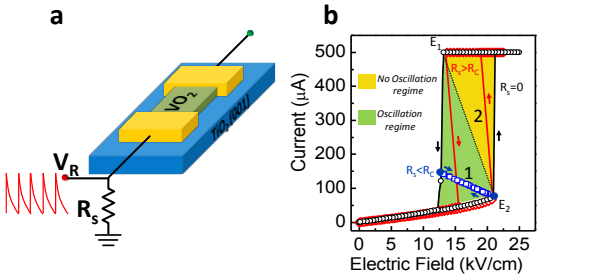


**Figure 1: Schematic of the circuit used to access the non-hysteretic transition regime in $VO_2$ via negative feedback generated by the series resistor Rs. The electric field across VO2 E = $(V_{in}$-VR)/$L_{VO2}$ plays a crucial role in the phase transition. (b) Current-electric field characteristics across $VO_2$ for different $R_s$. The external resistance $R_s$ modifies the $VO_2$ phase transition dynamics through negative feedback. A oscillation regime can be accessed using the appropriate $R_s$ (>RC). Electrical load lines for oscillatory (1) and non-oscillatory (2) regime are superimposed.**

across the phase transition with $R_s$=0 Ω (Figure 1b), the insulator-to-metal transition (IMT) and the metal-to-insulator transition (MIT) in $VO_2$ occur at two different critical electric fields, $E_2$ and $E_1$, respectively[19]. In other words, $E_2$ represents the critical point after which the metallic high conductivity phase in $VO_2$ is electrically stabilized while $E_1$ is the critical point at which the metallic phase no longer be electrically stabilized and the device returns to its high resistivity insulating state. These critical fields differ in magnitude giving rise to hysteresis.

In contrast to this hysteretic transition, a non-hysteretic transition can be induced by modifying the phase transition dynamics so that triggering the IMT (by surpassing $E_2$) results in a negative differential resistance (NDR) characterized by an increase in conductivity as well as a simultaneous reduction in electric field across the $VO_2$ device. If the field across the $VO_2$ now drops below the critical field $E_1$, it makes the high conductivity metallic phase unstable resulting in a spontaneous MIT. Representing this scenario through an electrical load line (Figure 1b), a $VO_2$ device operating on load line '1' will undergo a non-hysteretic transition, whereas a device operating on load line '2' will go through a hysteretic transition.

While the NDR and the load lines described above cannot be achieved using the $R_S$=0 Ω configuration, the addition of a simple $R_s$ in series makes this feasible. $R_s$ provides a stabilizing negative feedback compensating the positive internal feedback arising from the collective carrier dynamics as the $VO_2$ undergoes phase transition. This negative feedback modulates the current-electric field characteristics across the $VO_2$ and establishes the load line relation

$$E_{VO2} = E_2 - \frac{\Delta I_{VO2} R_s}{L_{VO2}} \quad (1)$$

where $\Delta I_{VO2} = I_{VO2}(E_{VO2}) - I_{VO2}(E_2)$ and $l_{VO2}$ is the $VO_2$ channel length. From equation (1), it is evident that $R_s$ tunes the $VO_2$ current-electric field characteristics and sets the criteria for non-hysteretic/hysteretic switching. The critical resistance $R_C$ that enables the non-hysteretic regime of operation ensures that the metallic phase is never completely stabilized and is given by

$$R_c \geq \frac{L_{VO2}}{W_{VO2} t_{VO2}} \left| \frac{E_2 - E_1}{\sigma_{SC} E_2 - \sigma_m E_1} \right| \quad (2)$$

where $W_{VO2}$ and $t_{VO2}$ are the $VO_2$ channel width and thickness, respectively, and $\sigma_m$ and $\sigma_{sc}$ are the equivalent insulating and metallic state conductivities, respectively.

Further, the conductivity in the NDR regime as indicated by $\Delta I_{VO2}$ is tuned by the electric field (equation (1)) with conductivity increasing as the electric field drops (and vice-versa). Such a system will oscillate (Figure 1c) if the conductivity and the electric-field across the device modulate each other in a way that the field driven restoring force enables the system to trace the same electrical trajectory periodically[20]. This criterion is fulfilled only in the non-hysteretic operating regime and results in sustained oscillations when $R_s > R_c$. Hence, harnessing the correlated physics in $VO_2$ using appropriate circuit elements allows us to realize relaxation oscillations in $VO_2$.

## 5. OSCILLATION DYNAMICS AND SCALING

The time domain waveform of the $VO_2$ oscillator (Figure 2a; single time period shown as inset) shows an exponential voltage buildup and decay (across $R_s$) associated with MIT and IMT in $VO_2$ respectively and is characterized by two R-C time constants $\tau_1$ and $\tau_2$ (see inset Figure 2a) which primarily control the oscillation frequency. $\tau_1$ (=0.35 μs), associated with the IMT is smaller than $\tau_2$

(=0.65 µs). The corresponding power spectrum for the oscillations is shown in Figure 2b. The exponential nature of the time domain waveform results in a gradual decay of the frequency harmonics and therefore the first harmonic is only ~10dB below the fundamental frequency (not shown here). The power distribution in the harmonics may be altered using a voltage controlled external

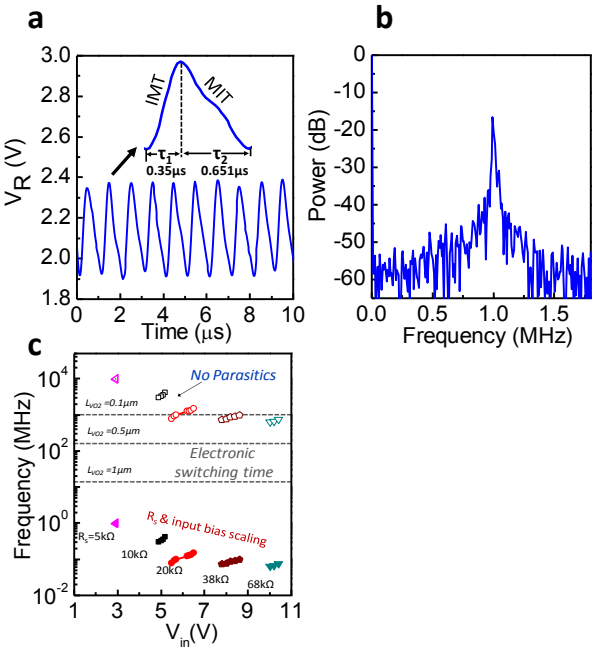


**Figure 2: (a) Time domain waveform of the $VO_2$ relaxation oscillator (Inset) shows the waveform for one oscillation period with the two time constants ($\tau_1$ and $\tau_2$) associated with IMT and MIT. $\tau_2$ (= 0.651 µs) is larger than $\tau_1$ (= 0.35 µs) (b) Power spectrum (power expressed as mean square amplitude in dB) of the oscillator. (c) Frequency scaling of the $VO_2$ relaxation oscillator. The frequency increases as the external $R_s$ is scaled down. The device resistance has also been scaled to further increase the output frequency. The unfilled symbols project the effect of eliminating parasitic elements. The dimension dependent electronic time constants (grey lines) will ultimately limit $f_{osc}$.**

resistance $R_s$.

Further, we study the oscillator frequency ($f_{osc}$) and dimensional scalability, which is crucial to implementing dense, large scale $VO_2$ oscillator circuits. Since $f_{osc}$ is set by the RC time constant of the oscillator circuit, we explore $f_{osc}$ scaling with $R_S$ (Figure 2c). As $R_s$ is reduced, frequencies up to 1 MHz are experimentally realized. The R-C time constants $\tau_1$ =0.35 µs and $\tau_2$ =0.35 µs for the $f_{osc}$=1MHz case are much larger than the intrinsic electronic switching time[21] associated with the phase transition in $VO_2$ and therefore there is ample scope for device and frequency scaling. All experiments in this work are performed using discrete components (resistors) and eliminating the parasitic elements associated with the present wiring schemes through monolithic integration as well as device scaling [22] will increase $f_{osc}$.

## 6. COUPLED $VO_2$ OSCILLATORS – EXPERIMENTAL DEMONSTRATION

The realization of inductor free, compact and scalable nonlinear oscillatory systems using $VO_2$ portends non-Boolean computing architectures based on the synchronization dynamics of such oscillators, provided we identify a coupling mechanism. Long range electrical charge based coupling is crucial to implementing large oscillator arrays compared to other state-variables (like spin), which may have limited coherence length at room temperature.

Figure 3a shows a schematic of the coupled oscillator circuit. Prior to coupling, the two individual $VO_2$ oscillators frequencies are, $f_{osc,1}$=48.43 kHz and $f_{osc,2}$=37.27 kHz (Figure 3b), which are set by using appropriate $R_s$ values: $R_{s1}$=38kΩ (6$R_c$) and $R_{s2}$=47kΩ (7.5$R_c$). After the oscillators are capacitively coupled ($C_C$=680 pF) they frequency lock and converge to a single resonant frequency (22.95 kHz). This is accompanied by a sharp narrowing of the spectral line width (Figure 3b). The reduced line-width after locking reflects the mutual feedback induced stabilization against noise [6], implying that the synchronized state is a highly stable configuration for the coupled system.

The use of capacitive coupling is motivated by the high pass filtering characteristics of the coupling configuration, which ensures that the individual oscillators can synchronize without mutually affecting their DC quiescent point. $C_C$ modifies the frequency dynamics of each oscillator through an effective coupling term $C_{eff}$:

$$C_{eff} = C_c C_1 + C_c C_2 + C_1 C_2 \quad (3)$$

where $C_1$ and $C_2$ are the net capacitances of each oscillator. $C_1$ and $C_2$ include the internal domain capacitances associated with each $VO_2$ film and device as well the parasitic elements. The $C_C$ element stores and dynamically redistributes reactive (non-dissipative) power between the oscillators facilitating synchronization.

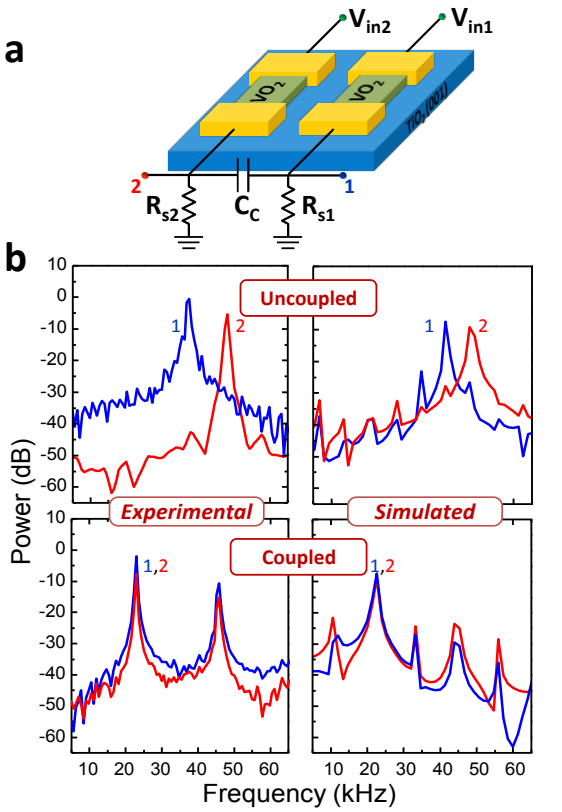


**Figure 3: (a) Schematic of two capacitively coupled $VO_2$ oscillators tuned to different oscillating frequencies with $R_{s1}$ = 38 kΩ (= 6$R_c$) and $R_{s2}$ = 47 kΩ (= 7.5$R_c$). (b) Experimental and simulated power spectrum (power expressed as mean square amplitude in dB) of both oscillators before and after coupling. The individual oscillator frequencies lock to a new frequency when coupled capacitively ($C_c$ = 680 pF).**

## 7. $VO_2$ BASED COUPLED OSCILLATORS

The experimental demonstration of $VO_2$ based coupled oscillator systems motivate theoretical understanding of their coupling dynamics. These systems are piecewise-linear [23] as opposed to having a single equation that describe their dynamics which makes their analysis difficult. In the following section, we will present a simplified view of the coupling dynamics with particular emphasis on the phase locking properties of such oscillators. Due to a finite capacitance being associated with the $VO_2$ films in their insulating phase, the voltage across the device builds up until the insulator-to-metal (IMT) phase transition occurs. The transition to metal forces the capacitor to discharge, resulting in a current through the series resistor, increasing the voltage across it (and hence, decreasing the voltage across the $VO_2$ device). This decrease, when sufficient, causes the metal-to-insulating (MIT) phase transition. This causes the cycle to repeat resulting in sustained oscillations. When capacitively coupled, such systems of oscillators tend to lock if their initial frequency difference is within the locking range. Controlling the series resistance can control the frequency of such an oscillator. In this paper we demonstrate that once locked a pair of coupled relaxation oscillators tend to antilock in phase (i.e., 180 degrees apart) and we propose to use such frequency control in a template matching problem.

## 8. SYSTEM MODEL

### 8.1 Single Oscillator

Before proceeding further, let us investigate the mathematical models describing the pairwise coupled system. Let the following parameters be defined for the $VO_2$ device:

- $g_i$ - internal conductance of the device in insulating phase
- $g$ - internal conductance of the device in metallic phase
- $g_s$- conductance of the series resistance
- $c$ - internal capacitance of the device

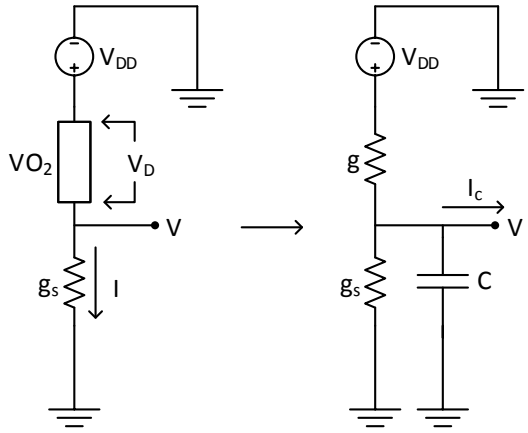


**Figure 4: $VO_2$ oscillator and its equivalent circuit**

Figure 4 shows the equivalent circuit of this configuration. The dynamics of a single oscillator comprising of a $VO_2$ device in series with a series conductance $g_s$ can be described by the following set of ODEs:

$$\begin{array}{ll} cv' = -g_c v + g_c v_{dd} & for\ charging \\ cv' = -g_d v & for\ discharging \end{array} \quad (4)$$

Here $g_c$ is the effective charging conductance of the system, and $g_d$ the discharging conductance. The device is in metallic phase during charging, and in insulating phase during discharging. When $g_i \ll g_s$ and $g \gg g_s$, the effective conductances can be approximated by $g_c \cong g$ and $g_d \cong g_s$. In the rest of the paper this approximation will be used, giving rise to the following ODEs:

$$\begin{array}{ll} cv' = -gv + gv_{dd} & for\ charging \\ cv' = -g_s v & for\ discharging \end{array} \quad (5)$$

### 8.2 Frequency Control

The frequency of the oscillatory system can be controlled by controlling the series resistance. In a possible monolithic implementation, the series resistance will be replaced by a MOSFET whose gate voltage can be used as a control mechanism to control the resultant series resistance and hence the dynamical behavior of the overall system. The voltage swing of the oscillator is assumed to be such that it keeps the transistor in saturation mode. The small signal analysis (Figure 5) of this circuit yields the following modified voltage equation:

$$\begin{array}{ll} cv' = -gv + gv_{dd} & for\ charging \\ cv' = -g_0 v - g_m v_{gs} & for\ discharging \end{array} \quad (6)$$

The variation of frequency of such an oscillator system with $v_{gs}$ is shown in Figure 6 and it demonstrates strong $v_{gs}$ dependence.

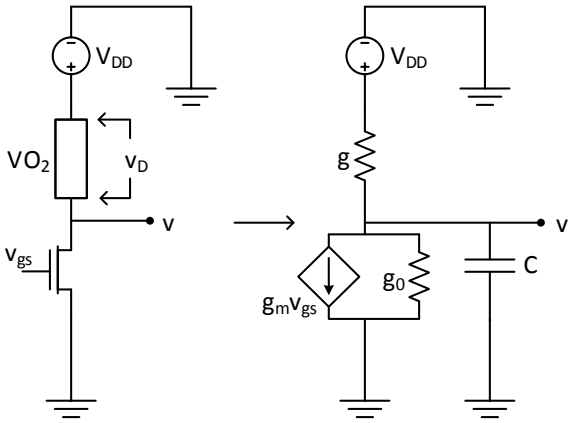


**Figure 5: $VO_2$ oscillator with a series transistor and its small signal equivalent circuit**

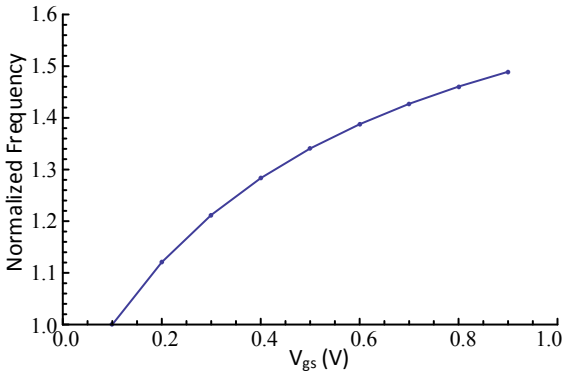


**Figure 6: Variation of frequency (normalized to the frequency at $V_{gs}$ = 0.1) with gate voltage $V_{gs}$**

### 8.3 Coupled systems and synchronization

When such oscillators are coupled using a capacitor, closer frequencies tend to lock out of phase (Figure 7) and frequencies that are far away do not. This can be easily seen in the phase diagrams of Figure 8. We use an averaged XOR measure for testing whether the oscillators have locked or not. Figure 9 shows the variation of

averaged XOR output of the oscillators with varying gate voltages applied on the transistors.

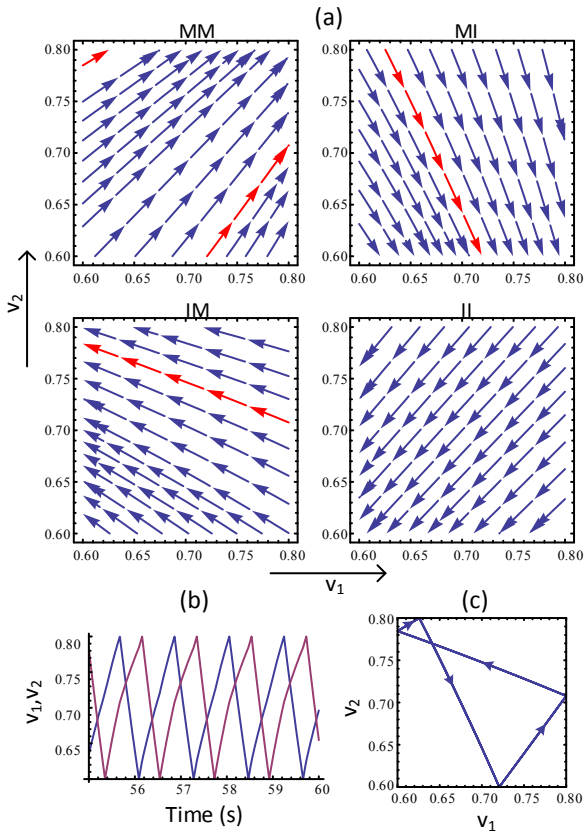


**Figure 7: (a) Phase diagrams in 4 phase combinations - MM, MI, IM, II. Red curve show the trajectory in steady state. (b) Time domain waveforms in steady state (c) Combined phase domain steady state trajectory. When locked, the system in the steady state mostly has a butterfly shaped trajectory and avoids the I-I phase as seen in (a). In the transients of locked case and in no-locking case, the system does enter I-I phase.**

As can be seen in the figure, the XOR surface is very similar to $(x-y)^2$ surface in the region of locking, and hence can be used as a method of frequency comparison. In the next section, we demonstrate the use of such circuits in template matching.

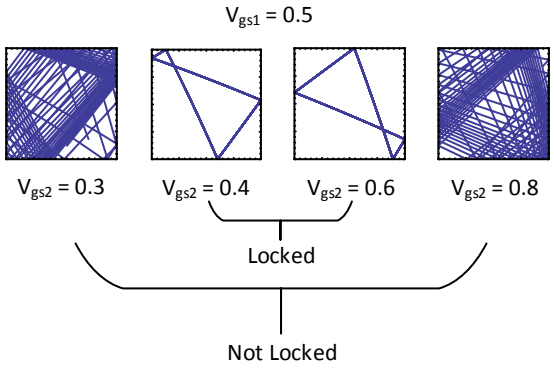


**Figure 8: Phase diagrams for various $V_{gs2}$ values with $V_{gs1}$ fixed at 0.5. The system locks for $V_{gs2}$ closer to $V_{gs1}$**

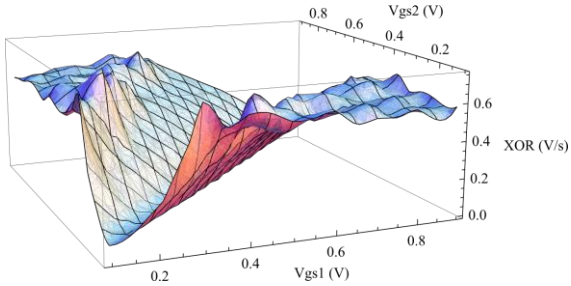


**Figure 9: Surface plot of averaged XOR output for different values of $V_{gs1}$ and $V_{gs2}$**

## 9. TEMPLATE MATCHING

For demonstrating the application of coupled $VO_2$ based relaxation oscillators in template matching, we use arrays of such oscillators and apply individual values of patterns as analog voltages to the gates of the transistors of individual oscillators in the array. This configuration in effect achieves a kind of FSK of the patterns. Each oscillator in the array is coupled to the respective oscillator in a template array (to be matched against), whose gate nodes are supplied analog voltages of stored template pattern values. The XOR outputs of each coupled system is then thresholded, and maximum number of matches in a pattern is considered a match in a winner-take-all fashion. Figure 10 depicts such a system for matching two patterns.

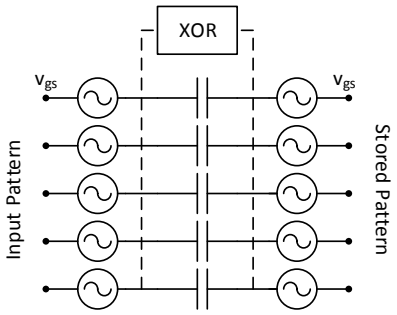


**Figure 10: The system for pattern matching using VO2 coupled oscillators**

Such a system is applied for matching faces (Figure 11) and handwritten number patterns (Figure 12). The color on each square demonstrates the degree of match and it can be easily seen that for template matching the proposed system performs with very high accuracy. It should be noted that in a variety of pattern matching problems, an important step is the feature extraction and it has not been discussed here. However in applications where template matching is required (e.g., digitizing printed books or identifying pictures in a large database) such a simple computational paradigm can be a powerful model of computing Euclidean distances using the attractor properties of nonlinear dynamical systems.

## 10. CONCLUSIONS

In this paper we demonstrate the use of synchronous $VO_2$ based oscillatory systems for neuro-morphic pattern recognition and template matching. Through experimental results and theoretical analysis such systems have been shown to use the attractor properties of synchronous oscillations to antilock in phase. We have harnessed that to realize template matching as one possible computational paradigm.

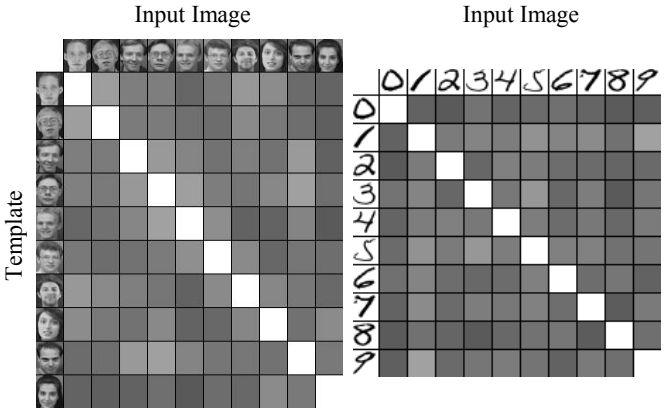


**Figure 11: XOR outputs for matching faces (left) and handwritten number patterns (right) using coupled $VO_2$ oscillators. White represents low XOR output, i.e. a good match.**


## Acknowledgements

This work was supported by Office of Naval Research Basic Research Challenge (BRC) through award N00014-11-1-0665 and by National Science Foundation Expeditions in Computing Award: 1317560. We thank Dr. Hanjong Paik and Prof. Darrell G. Schlom at Cornell University for growing the epitaxial $VO_2$ films. Abhinav Parihar and Arijit Raychowdhury would like to acknowledge the generous gift of Intel Corporation which made this work possible.


## 11. REFERENCES


[1] E. M. Izhikevich, "Computing with oscillators," 2000.

[2] T. Roska, A. Horvath, A. Stubendek, F. Corinto, G. Csaba, W. Porod, T. Shibata, and G. Bourianoff, "An Associative Memory with oscillatory CNN arrays using spin torque oscillator cells and spin-wave interactions architecture and End-to-end Simulator," in 2012 13th International Workshop on Cellular Nanoscale Networks and Their Applications (CNNA), 2012, pp. 1–3.

[3] T. Shibata, R. Zhang, S. P. Levitan, D. E. Nikonov, and G. I. Bourianoff, "CMOS supporting circuitries for nano-oscillator-based associative memories," in 2012 13th International Workshop on Cellular Nanoscale Networks and Their Applications (CNNA), 2012, pp. 1–5.

[4] S. P. Levitan, Y. Fang, D. H. Dash, T. Shibata, D. E. Nikonov, and G. I. Bourianoff, "Non-Boolean associative architectures based on nano-oscillators," in 2012 13th International Workshop on Cellular Nanoscale Networks and Their Applications (CNNA), 2012, pp. 1–6.

[5] G. Csaba, M. Pufall, D. E. Nikonov, G. I. Bourianoff, A. Horvath, T. Roska, and W. Porod, "Spin torque oscillator models for applications in associative memories," in 2012 13th International Workshop on Cellular Nanoscale Networks and Their Applications (CNNA), 2012, pp. 1–2.

[6] S. Kaka, M. R. Pufall, W. H. Rippard, T. J. Silva, S. E. Russek, and J. a Katine, "Mutual phase-locking of microwave spin torque nano-oscillators.," Nature, vol. 437, no. 7057, pp. 389–92, Sep. 2005.

[7] L. A. Ladd and W. Paul, "Optical and transport properties of high quality crystals of $V_2O_4$ near the metallic transition temperature," Solid State Commun., vol. 7, no. 4, pp. 425–428, Feb. 1969.

[8] M. M. Qazilbash, M. Brehm, B.-G. Chae, P.-C. Ho, G. O. Andreev, B.-J. Kim, S. J. Yun, a V Balatsky, M. B. Maple, F. Keilmann, H.-T. Kim, and D. N. Basov, "Mott transition in $VO_2$ revealed by infrared spectroscopy and nano-imaging.," Science, vol. 318, no. 5857, pp. 1750–3, Dec. 2007.

[9] B.-J. Kim, Y. Lee, S. Choi, J.-W. Lim, S. Yun, H.-T. Kim, T.-J. Shin, and H.-S. Yun, "Micrometer x-ray diffraction study of $VO_2$ films: Separation between metal-insulator transition and structural phase transition," Phys. Rev. B, vol. 77, no. 23, p. 235401, Jun. 2008.

[10] H.-T. Kim, B.-G. Chae, D.-H. Youn, S.-L. Maeng, G. Kim, K.-Y. Kang, and Y.-S. Lim, "Mechanism and observation of Mott transition in $VO_2$-based two- and three-terminal devices," New J. Phys., vol. 6, pp. 52–52, May 2004.

[11] A. Cavalleri, C. Tóth, C. Siders, J. Squier, F. Ráksi, P. Forget, and J. Kieffer, "Femtosecond Structural Dynamics in $VO_2$ during an Ultrafast Solid-Solid Phase Transition," Phys. Rev. Lett., vol. 87, no. 23, p. 237401, Nov. 2001.

[12] J. Cao, E. Ertekin, V. Srinivasan, W. Fan, S. Huang, H. Zheng, J. W. L. Yim, D. R. Khanal, D. F. Ogletree, J. C. Grossman, and J. Wu, "Strain engineering and one-dimensional organization of metal-insulator domains in single-crystal vanadium dioxide beams.," Nat. Nanotechnol., vol. 4, no. 11, pp. 732–7, Nov. 2009.

[13] A. Zylbersztejn, "Metal-insulator transition in vanadium dioxide," Phys. Rev. B, vol. 11, no. 11, pp. 4383–4395, Jun. 1975.

[14] T. M. Rice and J. P. Pouget, "Comment on '$VO_2$: Peierls or Mott-Hubbard? A View from Band Theory'," Phys. Rev. Lett., vol. 73, no. 22, pp. 3042–3042, Nov. 1994.

[15] R. M. Wentzcovitch, "$VO_2$: Peierls or Mott-Hubbard? A view from band theory," Phys. Rev. Lett., vol. 72, no. 21, pp. 3389–3392, May 1994.

[16] A. Cavalleri, T. Dekorsy, H. Chong, J. Kieffer, and R. Schoenlein, "Evidence for a structurally-driven insulator-to-metal transition in $VO_2$: A view from the ultrafast timescale," Phys. Rev. B, vol. 70, no. 16, p. 161102, Oct. 2004.

[17] V. Eyert, "$VO_2$: A Novel View from Band Theory," Phys. Rev. Lett., vol. 107, no. 1, p. 016401, Jun. 2011.

[18] Z. Yang, C. Ko, and S. Ramanathan, "Oxide Electronics Utilizing Ultrafast Metal-Insulator Transitions," Annu. Rev. Mater. Res., vol. 41, no. 1, pp. 337–367, Aug. 2011.

[19] N. Sugimoto, S. Onoda, and N. Nagaosa, "Field-induced metal-insulator transition and switching phenomenon in correlated insulators," Phys. Rev. B, vol. 78, no. 15, p. 155104, Oct. 2008.

[20] C. J. Hu, "Self-sustained oscillation in an $R_H$-C or $R_H$-L circuit containing a hysteresis resistor $R_H$" IEEE Trans. Circuits Syst., vol. 33, no. 6, pp. 636–641, Jun. 1986.

[21] A. Kar, N. Shukla, E. Freeman, H. Paik, H. Liu, R. Engel-Herbert, S. S. N. Bharadwaja, D. G. Schlom, and S. Datta, "Intrinsic electronic switching time in ultrathin epitaxial vanadium dioxide thin film," Appl. Phys. Lett., vol. 102, no. 7, p. 072106, 2013.

[22] M. D. Pickett and R. S. Williams, "Sub-100 fJ and sub-nanosecond thermally driven threshold switching in niobium oxide crosspoint nanodevices" Nanotechnology, vol. 23, no. 21, p. 215202, Jun. 2012.

[23] T. Saito, "On a coupled relaxation oscillator," IEEE Trans. Circuits Syst., vol. 35, no. 9, pp. 1147–1155, 1988.